



# The association of defensin HNP-2 with negatively charged membranes: A combined fluorescence and linear dichroism study



Catherine J. Pridmore<sup>a</sup>, Alison Rodger<sup>b</sup>, John M. Sanderson<sup>a,\*</sup>

<sup>a</sup> Chemistry Department, Durham University, Durham DH1 3LE, UK

<sup>b</sup> Department of Chemistry, University of Warwick, Coventry CV4 7AL, UK

## ARTICLE INFO

### Article history:

Received 2 October 2015

Received in revised form 11 January 2016

Accepted 19 January 2016

Available online 20 January 2016

### Keywords:

Antibiotic peptide

Lipid membrane

Linear dichroism

Fluorescence

Binding

Kinetics

## ABSTRACT

The association of defensin HNP-2 with negatively charged membranes has been studied using a new approach that combines fluorescence and linear dichroism (LD) spectroscopies with simulated LD spectra in order to characterise the binding kinetics and bound configurations of the peptide. Binding to membranes composed of mixtures of diacylglycerophosphocholines (PC) with either diacylglycerophosphoglycerol (PG) or diacylglycerophosphoserine (PS) was conducted at lipid:peptide ratios that yielded binding, but not membrane fusion. HNP-2 association with membranes under these conditions was a 2 stage-process, with both stages exhibiting first order kinetics. The fast initial step, with a half-life of  $< 1$  min, was followed by a slower step with a half-life of  $> 3$  min. Conversion between the states was estimated to have an enthalpy of activation of approximately  $10 \text{ kJ mol}^{-1}$  and an entropy of activation of  $-0.2 \text{ kJ K mol}^{-1}$ . LD spectra corresponding to each of the membrane bound states were generated by non-linear regression using a standard kinetic model. These spectra are interpreted in comparison with spectra calculated using the program Dichrocalc and reveal that the peptide associates with membranes in a small number of stable configurations. All of these configurations have a significant proportion of  $\beta$ -sheet structure residing in the plane of the membrane. Two configurations support structures previously proposed for defensins in membranes.

© 2016 The Authors. Published by Elsevier B.V. This is an open access article under the CC BY license (<http://creativecommons.org/licenses/by/4.0/>).

## 1. Introduction

Defensins are arginine-rich cationic peptides with molecular weights of 3–5 kDa which adopt predominantly  $\beta$ -sheet structures stabilised by 3–4 disulfide bonds [1–3]. There are six  $\alpha$ -defensins: human neutrophil peptides 1–4 (HNP-1–4) and human defensins 4 and 5 (HD-5, HD-6) [4]. HNP-1–3 have primary structures that only differ by a single residue at the N-terminus [5]. These defensins adopt a three-stranded antiparallel  $\beta$ -sheet structure [6] stabilised by six cysteine residues, paired Cys1–Cys6, Cys2–Cys4 and Cys3–Cys5 (where the numbers reflect the relative position in the sequence, not residue numbers) [7,8]. The crystal structures of all six human  $\alpha$ -defensins have been determined, although in the case of HNP-2, the second glycine (Gly16) was replaced with D-Ala. Solid and solution state NMR structures are also available for HNP-1 [6,9–14]. All of the human  $\alpha$ -defensins crystallise as dimers, and solid state NMR analysis of HNP-1 also shows it to have a dimeric structure [14]. The secondary structures

of HNP-1–3 have been shown to be essentially identical, with three strands of antiparallel  $\beta$ -sheet, and only show small differences in the sections where no specific secondary structure can be assigned (Fig. 1) [6,9,13]. It is believed that defensins act through permeabilisation of microbial cell membranes causing leakage of the contents [15–18]. HNP-2 has a net charge of +3 at pH 7, making it unsurprising that the peptide will bind to lipid bilayers containing a proportion of negatively charged lipids, due to electrostatic attractions [19]. The extent of binding of HNP-2 to vesicles composed of negatively charged 1-palmitoyl-2-oleoyl-*sn*-glycero-3-phosphocholine (POPG) and neutral 1-palmitoyl-2-oleoyl-*sn*-glycero-3-phosphocholine (POPC) has been shown by equilibrium dialysis to have a sigmoidal dependency on the concentration of POPG. No binding was observed in the absence of POPG. Approximately 20% binding of HNP-2 was observed with 10 mol% POPG at a total lipid concentration of 10 mM, increasing to approximately 60% with 20 mol% POPG. Maximum binding (at around 90%) did not occur until the content of negatively charged lipid was around 70 mol%, although due to the sigmoidal nature of the binding curve, the extent of binding at 50 mol% POPG was only marginally lower [20].

After binding, it has been shown that HNP-2 causes lysis of the membrane. This has been observed both with negatively charged vesicles and with the inner and outer membranes of *Escherichia coli* [22,23]. HNP-2 has also been shown to cause fusion and aggregation of vesicles under certain conditions. Aggregation occurs at low total lipid

Abbreviations: CD, circular dichroism; DMPC, 1,2-dimyristoyl-*sn*-glycero-3-phosphocholine; DMPG, 1,2-dimyristoyl-*sn*-glycero-3-phosphoglycerol; DOPC, 1,2-dioleoyl-*sn*-glycero-3-phosphocholine; DOPS, 1,2-dioleoyl-*sn*-glycero-3-phosphoserine; HNP, human neutrophil peptide; LD, linear dichroism; POPG, 1-palmitoyl-2-oleoyl-*sn*-glycero-3-phosphoglycerol.

\* Corresponding author.

E-mail address: [j.m.sanderson@durham.ac.uk](mailto:j.m.sanderson@durham.ac.uk) (J.M. Sanderson).



**Fig. 1.** The DSSP [21] secondary structure assignment of HNP-2 (PDB ID: 1ZMH) [9].  $\beta$  strands are shown by red arrows,  $\beta$  turns in blue, sections with no secondary structure assigned in black (—) and bridged cysteines by green lines. The D-Ala residue shown in bold (Ala16) is a Gly in the native HNP-2 structure.

concentrations with vesicles containing at least 40 mol% POPG and 60 mol% POPE. With pure POPG liposomes, aggregation is rapid when the molar ratio of POPG lipid to HNP-2 is below 100:1, which suggests that the aggregation is caused by electrostatic interactions [22]. HNP-1 has been observed to cause fusion of liposomes containing 25% DOPS in DPPC [18]. The activity of HNPs is strongly affected by the ionic strength of the medium [18]. Membrane binding is weaker at high ionic strengths (also consistent with the electrostatic nature of the interaction), with the consequence that the lytic activity disappears and the fusion activity is significantly reduced. The antimicrobial activity of HNP-1 against Gram negative (*E. coli*) and Gram positive (*Listeria monocytogenes*) bacteria is similarly significantly inhibited by buffers of even medium ionic strength [24]. A number of models have been proposed to account for HNP activity, ranging from an active membrane-associated dimer, through two-dimer models, to multiple dimer pores [6,22]. However, direct structural and spectroscopic studies on the assembly intermediates in the membrane, and the rate at which they form have not been conducted.

Oriented circular dichroism (CD) [25,26] and linear dichroism (LD) [27] methodologies can provide information on the conformation and alignment of peptides in membranes. LD shows the orientation of electronic transitions with respect to the experimental frame of reference. In membranes aligned by shear flow [28,29] in a Couette cell [30,31], LD yields information on both the kinetics [32,33] of membrane association and the alignment [33,34] of the peptides with respect to the membrane, with the advantage that the unbound peptide does not align and therefore does not produce any LD. In this paper we determine the kinetics of HNP-2 association with membranes using fluorescence and linear dichroism spectroscopies, combined with studies on the aggregation behaviour of the liposomes in the presence of the peptide. From the LD data in particular, we are able to analyse the alignment of the membrane-bound peptide and thus assess the binding models proposed in the literature.

## 2. Materials and methods

### 2.1. Materials

1,2-Dioleoyl-*sn*-glycero-3-phosphocholine (DOPC) and 1,2-dioleoyl-*sn*-glycero-3-phosphoserine (DOPS) were obtained from Sigma-Aldrich. 1,2-Dimyristoyl-*sn*-glycero-3-phosphocholine (DMPC) was purchased from Bachem (UK) Ltd., St. Helens, UK. 1-Palmitoyl-2-oleoyl-*sn*-glycero-3-phosphoglycerol (POPG) was obtained from Avanti Polar Lipids through Instruchemie B.V., The Netherlands. DMPC was Alexis brand, obtained from Enzo Life Sciences (UK) Ltd., Exeter, UK. Defensin human neutrophil peptide-2 (HNP-2) was obtained from Bachem (UK) Ltd., St. Helens, UK.

### 2.2. Liposome preparation

Liposomes were prepared by evaporation of a solution of the lipid in  $\text{CHCl}_3$  or  $\text{CHCl}_3/\text{MeOH}$  (10:2 (v/v)) to a thin film inside a round bottomed flask in vacuo. Lipid films were placed in a vacuum desiccator for a minimum of 2 h before the addition of water or buffer. The flask was then vortexed and 5 freeze–thaw cycles carried out using liquid nitrogen and warm water. The lipid suspensions were extruded 10 times through laser-etched polycarbonate membranes (Whatman) with 100 nm pores using a LIPEX thermobarrel extruder (Northern Lipids

Inc., BC, Canada). The extruder was warmed to a temperature (typically 50 °C) above the phase transition temperature of the lipids being prepared.

### 2.3. Peptide concentration

The HNP-2 concentration was determined by the absorbance at 280 nm following serial addition of small volumes of peptide to a water blank and determination of the stock concentration by linear regression using an extinction coefficient of  $\epsilon_{280} = 10,345 \text{ M}^{-1} \text{ cm}^{-1}$  [35].

### 2.4. HNP-2 monomer–dimer equilibrium

Data for monomer–dimer equilibrium analysis were obtained using an ISA Jobin-Yvon Spex Fluorolog-3 luminescent spectrometer (Horiba Jobin Yvon Ltd., Middlesex, UK) with an array photon multiplier tube using DataMax v2.20 software. The data for 1–39  $\mu\text{M}$  HNP-2 were collected by adding 30 aliquots of 2  $\mu\text{L}$  HNP-2 to 60  $\mu\text{L}$   $\text{H}_2\text{O}$ . Two spectra were recorded after each addition with the results averaged. For the lower concentration range, a solution of 1.5  $\mu\text{M}$  HNP-2 was increasingly diluted by the addition of  $\text{H}_2\text{O}$  and the data from two spectra averaged at each concentration. All analyses were carried out with an excitation wavelength of 280 nm, 3 nm excitation and emission bandwidths and a 3 mm pathlength. Data were analysed according to the change in emission intensity at 325 nm as a function of total HNP-2 concentration. Least squares regression was performed using the Solver function in the program Excel (Microsoft, Redmond, WA) to fit Eq. (1) to the data:

$$F_{\text{calc}} = \frac{2K_a[\text{HNP} - 2]^2(F_d - F_m)}{[\text{HNP} - 2]_0} + F_m \quad (1)$$

where  $[\text{HNP}]_0$  is the total peptide concentration,  $K_a$  is the association constant,  $F_{\text{calc}}$  is the calculated fluorescence intensity, and  $F_d$  and  $F_m$  are the fluorescence intensities of the dimer and monomer respectively. The concentration of the dimeric species,  $[\text{HNP} - 2]_2$ , was determined using Eq. (2):

$$[\text{HNP} - 2]_2 = \frac{1 + 4K_a[\text{HNP} - 2]_0 - \sqrt{(1 + 8K_a[\text{HNP} - 2]_0)}}{8K_a} \quad (2)$$

With knowledge of  $[\text{HNP} - 2]_2$  and  $[\text{HNP}]_0$ , the concentration of free peptide,  $[\text{HNP} - 2]$  was calculated from the concentration balance.

### 2.5. HNP-2 membrane binding kinetics

Fluorescence measurements were conducted using a Jasco FP-6500 fluorimeter (Jasco UK, Great Dunmow, UK) with 2.5 nm excitation and emission bandwidths and a 3 mm pathlength. Samples were analysed at 2.5 min intervals for 5 h with a scan speed of 200 nm/min with excitation at 280 nm and a 3 mm pathlength. LD measurements were performed using a Jasco J-815 spectropolarimeter (Jasco UK) using Jasco Spectra Manager version 1.5 software, in a microvolume Couette flow cell (Crystal Precision Optics, Rugby, UK; now available from Kromatek Ltd., Great Dunmow, UK) [30]. The Couette cell was rotated at ~3000 rpm (3.0 V). Spectra were recorded at 5 min intervals over 5 h at a scan speed of 50 nm/min with a response time of 2 s and a data pitch of 0.2 nm. Data were analysed using a three-state model for the binding kinetics using Eq. (3):

$$LD_{\text{calc}} = \left( LD_{m1} \frac{[P_{m1}]}{[P]_0} \right) + \left( LD_{m2} \frac{[P_{m2}]}{[P]_0} \right) \quad (3)$$

where  $P_{m1}$  and  $P_{m2}$  are respectively the first and second membrane-associated states that form and  $[P]_0$  is the total peptide concentration.  $LD_{m1}$  and  $LD_{m2}$  represent the magnitude of the LD for the  $P_{m1}$  and  $P_{m2}$

states respectively. A similar approach was used for fluorescence emission data following HNP-2 addition to membranes (Eq. (4)):

$$F_{\text{calc}} = \left( F_f \frac{[P_f]}{[P]_0} \right) + \left( F_{m1} \frac{[P_{m1}]}{[P]_0} \right) + \left( F_{m2} \frac{[P_{m2}]}{[P]_0} \right) \quad (4)$$

where  $F_{m1}$  and  $F_{m2}$  represent the molar fluorescence of the  $P_{m1}$  and  $P_{m2}$  states respectively, and  $F_f$  is the fluorescence of the free peptide. For both models, the concentrations of the  $P_{m1}$  and  $P_{m2}$  states were obtained using Eqs. (5) and (6):

$$[P_{m1}] = \frac{[P]_0 k_1 (e^{-k_1 t} - e^{-k_2 t})}{k_2 - k_1} \quad (5)$$

$$[P_{m2}] = [P]_0 \left( 1 + \frac{k_1 e^{-k_2 t} - k_2 e^{-k_1 t}}{k_2 - k_1} \right) \quad (6)$$

where  $k_1$  is the rate of the first process that forms  $P_{m1}$  and  $k_2$  is the rate of conversion of  $P_{m1}$  to  $P_{m2}$ . The concentration of free peptide,  $P_f$  was calculated from the mass balance. Non-linear regression was conducted with least squares values weighted by  $1/t^2$ .

### 2.6. Calculated LD spectra

Model LD spectra of HNP-2 were obtained using Dichrocalc v3.3 software through the web interface (<http://comp.chem.nottingham.ac.uk/dichrocalc/>) [36–38]. A reference HNP-2 dimer structure was created from the PDB ID 1DFN using PyMol (version 0.99, OSX) to produce an approximate alignment of the peptide with the central  $\beta$ -sheet portion of the peptide in the  $x$ - $y$  plane. LD spectra were calculated in the reference orientation, and for incremental rotations  $\delta$  and  $\psi$  about the  $x$ -axis and  $y$ -axis respectively from the starting orientation up to  $90^\circ$ . For each of the two series of measurements, one angle was maintained at the reference value whilst the other was incremented. In order to take account of the fact that the peptide could bind in any orientation relative to rotation about the  $z$ -axis (corresponding to the membrane normal), and could be at any position around the surface of the shear-deformed liposome (assuming that the shape of this is cylindrical) a series of spectra obtained at  $30^\circ$  rotations about the  $z$ -axis and  $30^\circ$  tilt angles about the  $x$ -axis (corresponding to the long axis of the cylinder) was averaged for each starting structure. This was implemented in Dichrocalc by selecting the  $z$ -axis as the rotation axis and the  $x$ -axis as the tilt axis. The rationale for the axis system used is given in the appendix. The spectra resulting from these calculations were analysed mathematically according to Eqs. (7) and (8) for rotations  $\delta$  and  $\psi$  respectively:

$$LD_{\lambda,\delta}^r = \mu_{x,\lambda}^2 - \mu'_{\lambda,\delta} \cos^2(\alpha_{i,\delta} + \delta) + a_\lambda \quad (7)$$

$$LD_{\lambda,\psi}^r = \mu'_{\lambda,\psi} \cos^2(\alpha_{i,\psi} + \psi) - \mu_{y,\lambda}^2 + a_\lambda \quad (8)$$

where at any given wavelength  $\lambda$ ,  $\mu_{x,\lambda}$  is the component of the transition moment  $\mu$  along the  $x$ -axis (which is unchanged by rotations  $\delta$ ),  $\mu_{y,\lambda}$  is the component of the transition moment  $\mu$  along the  $y$ -axis (which is unchanged by rotations  $\psi$ ),  $\mu'_{\lambda,\delta}$  and  $\mu'_{\lambda,\psi}$  are the projections of the transition moment onto the  $x$ - $y$  plane in the laboratory frame,  $\alpha_{i,\delta}$  and  $\alpha_{i,\psi}$  are the angles subtended by the vector  $\mu$  with the  $y$ -axis and  $x$ -axis respectively in the reference state, and  $a_\lambda$  is a constant that reflects the anisotropic contribution from  $\mu_z$ . By conducting least squares regression to fit Eqs. (3) and (4) to the calculated LD data at each wavelength, all of the variables in these equations could be obtained. Over the wavelength range studied, these parameters enabled the LD response over a complete turn ( $2\pi$  radians) to be calculated using Eqs. (7) and (8), and the LD response for any combination of  $\delta$  and  $\psi$  over the wavelength range studied to be calculated using Eq. (9):

$$LD_\lambda = S' \left( \mu'_{\lambda,\psi} \cos^2(\alpha_{i,\psi} + \psi) - \mu'_{\lambda,\delta} \cos^2(\alpha_{i,\delta} + \delta) + a_\lambda \right) \quad (9)$$

where  $S'$  is a scaling factor that reflects the proportion of liposomes that are aligned as cylinders under shear flow, and a multiplication factor for conversion of reduced LD to LD. Least squares regression was used to fit Eq. (9) to the experimental LD spectra by optimising the values of  $\delta$  and  $\psi$ .

## 3. Results and discussion

### 3.1. Dimerisation of HNP-2

The equilibrium constant for HNP-2 dimerisation was determined by fluorescence spectroscopy in order that the aqueous-state oligomeric form of the peptide was known for membrane binding experiments. A series of fluorescence measurements was made in water on solutions of HNP-2 in order to study the self-association of the peptide. The tryptophan fluorescence spectrum of HNP-2 showed two emission maxima (ESI) at all concentrations down to the sensitivity limit of  $0.046 \mu\text{M}$ , with the emission maxima blue shifted relative to that of tryptophan in water. This suggests that two tryptophan populations exist within the HNP-2 solution. Analysis of the fluorescence intensity at 325 nm (Fig. 2) yielded a typical binding isotherm, with a calculated association constant ( $K_a$ ) for HNP-2 dimerisation of  $2.6 \times 10^5 \pm 2.8 \times 10^4 \text{ M}^{-1}$  ( $K_d = 3.8 \times 10^{-6} \pm 4 \times 10^{-7} \text{ M}^{-1}$ ). The moderate fit to the experimental fluorescence is understandable given the weak fluorescence emission of HNP-2 in this concentration range, but is nevertheless sufficient to estimate the proportion of dimer present in binding experiments with liposomes.

The two populations of tryptophan observed in the fluorescence spectra can be accounted for by studying the crystal structure of HNP-2 and the solid state NMR (ssNMR) structures of HNP-1 [14]. Each HNP-2 monomer contributes one tryptophan residue, three tyrosine residues and one phenylalanine residue to the dimer. The crystal structure of an HNP-2 dimer reveals that, although the backbone of the dimer is symmetrical, the two tryptophan side chains are not in equivalent environments relative to nearby tyrosine side chains, and that the tryptophan and tyrosine residues are close enough for excimer coupling to occur (Fig. 3). Similarly, two main tryptophan rotamers can be distinguished in the ssNMR structure of HNP-1, both of which are in close proximity to Tyr20 and Tyr2. There are therefore at least two low energy interactions between tryptophan and neighbouring tyrosine residues that can contribute to the fluorescence emission. Differences in the solvent exposure of the two tryptophan residues in the dimer are also likely to contribute to the observation of separate emission maxima, with the emission maximum of the less solvent exposed residue blue shifted relative to the other [39].

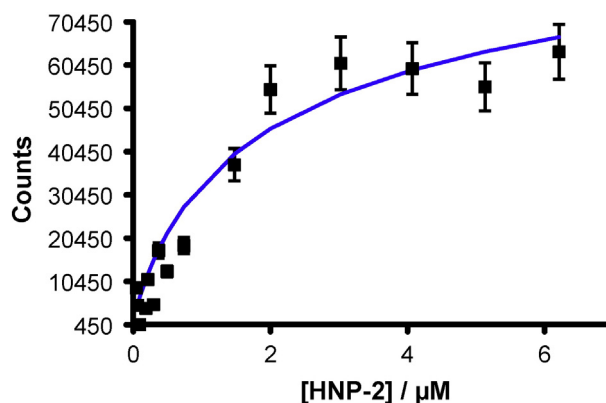
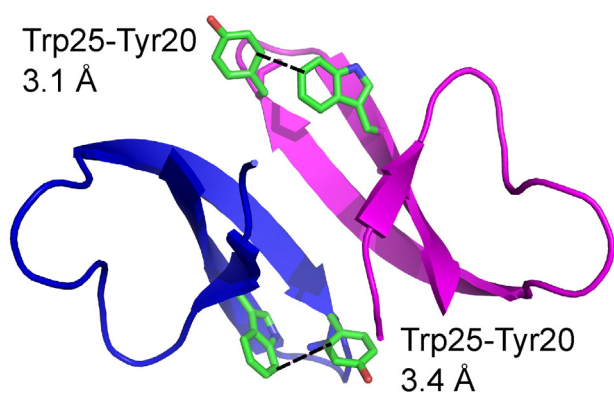


Fig. 2. Experimental and calculated fluorescence emission intensity of HNP-2 in water at 325 nm ( $\lambda_{\text{exc}} = 280 \text{ nm}$ ). Experimental data are presented as points and the profile calculated from non-linear regression as a line. Error bars are determined from repeat measurements.



**Fig. 3.** Structure of HNP-2 dimer (PDB ID: 1ZMH) [9] showing different orientations of tryptophan relative to neighbouring tyrosine residues and the closest C–C contact distances.

### 3.2. Conditions used for binding experiments

Liposome mixtures composed of 50:50 (w/w) negatively charged lipid and neutral PC were chosen for HNP-2 binding analyses in low salt buffers to maximise the extent of binding. For example, the extent of HNP-2 binding to membranes composed of 50:50 (w/w) POPG/POPC has been reported as 75% at a peptide concentration of 7.4  $\mu\text{M}$  and a total lipid concentration of 1 mM [20]. HNP-2 was used at a concentration of 15  $\mu\text{M}$  for our work as this was found to give good signal strength for LD and fluorescence measurements, with a lipid:peptide ratio of 100:1, and the extent of peptide-induced liposome aggregation at this ratio was expected to be minimal [22]. Under these conditions, the majority of the peptide in solution would be in the dimeric form at the start of the measurements. At these HNP-2 and lipid concentrations, no membrane fusion could be detected by either membrane incorporated FRET probes, or by dynamic light scattering (described in detail in the ESI).

### 3.3. Membrane binding measurements by fluorescence spectroscopy

The addition of HNP-2 to 50:50 (w/w) POPG/DOPC liposomes (Fig. 4A) yielded no blue-shift of the fluorescence maximum compared to the spectrum of the peptide in water. This can be attributed to a limited solvent exposure of the tryptophan residue in the dimer in solution, and the presence of an existing significant blue shift through interactions with neighbouring tyrosines. During the course of the lipid binding, the two emission maxima at 330 nm and 340 nm became more resolved. This suggests that in the membrane associated state, the tryptophan residues occupy well defined conformations in which one tryptophan–tyrosine contact is closer than the other, leading to a difference in exciton coupling. Extraction of the change in emission intensity at 330 nm (Fig. 4B) demonstrates an initial rise in emission intensity during the first hour, followed by a further rise in intensity before a drop in intensity at the end of the measuring period.

### 3.4. Membrane binding measurements by LD spectroscopy

LD spectra were obtained following HNP-2 addition to membranes composed of POPC/POPG, DOPS/DOPC and DMPC/DMPC (Fig. 5). Temperatures were selected to ensure that for membranes containing DOPC, experiments were conducted above the main gel to liquid crystal phase transition temperature ( $T_m$ ). For DMPC/DMPC membranes, experiments were conducted both above and below  $T_m$ .

For all membrane compositions there are clear changes in the intensities and profiles of the LD spectra over time, indicative of membrane binding events occurring on a timescale of seconds to minutes (the timescales of the experiments). The evolution of the LD profiles enabled

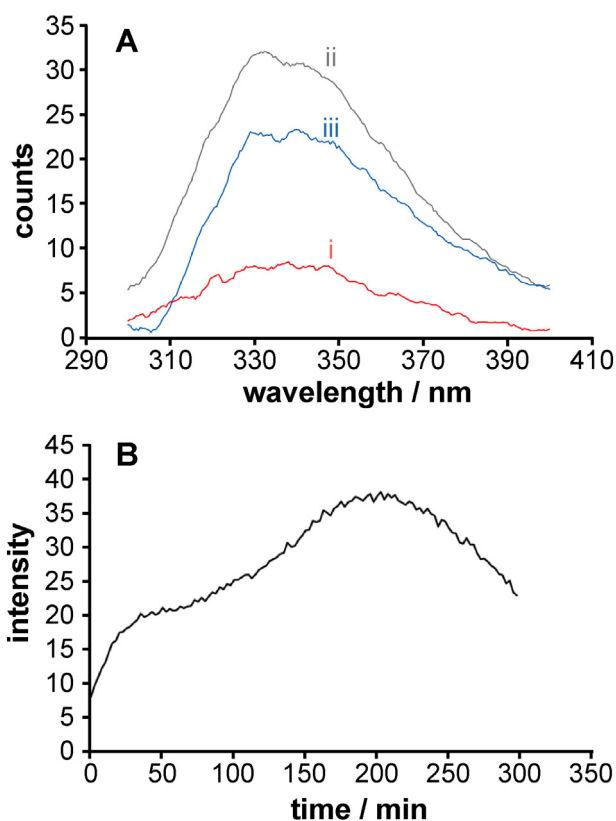


**Fig. 4.** A: Fluorescence spectra of HNP-2 recorded after 0 (i), 147.5 (ii) and 297.5 min (iii) following the addition of the peptide (15  $\mu\text{M}$ ) to 50:50 (w/w) POPG/DOPC liposomes (1.4 mM) at 30 °C.  $\lambda_{\text{exc}} = 280 \text{ nm}$ ; B: evolution of HNP-2 fluorescence emission intensity at 330 nm.

the binding kinetics to be determined (discussed below). Whilst the magnitudes of the LD changes for membranes containing DOPC as the neutral component were generally consistent, membranes containing DMPC yielded notable differences. In the case of the DMPC/DMPC mixture at 33 °C, a comparatively large LD evolved rapidly before relaxing to give LD with a magnitude comparable to the DOPC-based mixtures, suggesting that the initial membrane-associated form of HNP-2 in DMPC/DMPC membranes differs from the others. In the case of the DMPC/DMPC mixture at 17 °C, the spectrum contains evidence of scattering, although analysis of this mixture by other methods yielded no evidence for membrane fusion (see ESI). The scattering in the spectrum is attributed to the lipids being in the gel phase, as the intensity of light scattered from liposomes increases significantly below the phase transition temperature [40]. Even accounting for the scattering, this mixture yields by far the largest LD signals. CD spectra obtained over the same time period showed no evidence for changes in the conformation of HNP-2 in any of the membrane systems (see ESI). In general, all of the LD spectra are consistent with a  $\beta$ -sheet structure that is aligned parallel to the plane of the membrane, such as would be expected on the surface of the membrane, rather than inserted in a transmembrane alignment. A detailed analysis of the transitions is presented later in the article.

### 3.5. Analysis of binding kinetics

The fluorescence and linear dichroism data were modelled according to Scheme 1. This model includes the free peptide ( $P_f$ ) and two membrane associated states, denoted  $P_{m1}$  and  $P_{m2}$ . In the conditions of our experiments,  $P_f$  corresponds to the peptide dimer.

Semi-log plots of the evolution of the fluorescence intensity at 330 and 340 nm over the first 80 min (Fig. 6) suggested that the binding was pseudo-first order with respect to HNP-2. From the gradients of

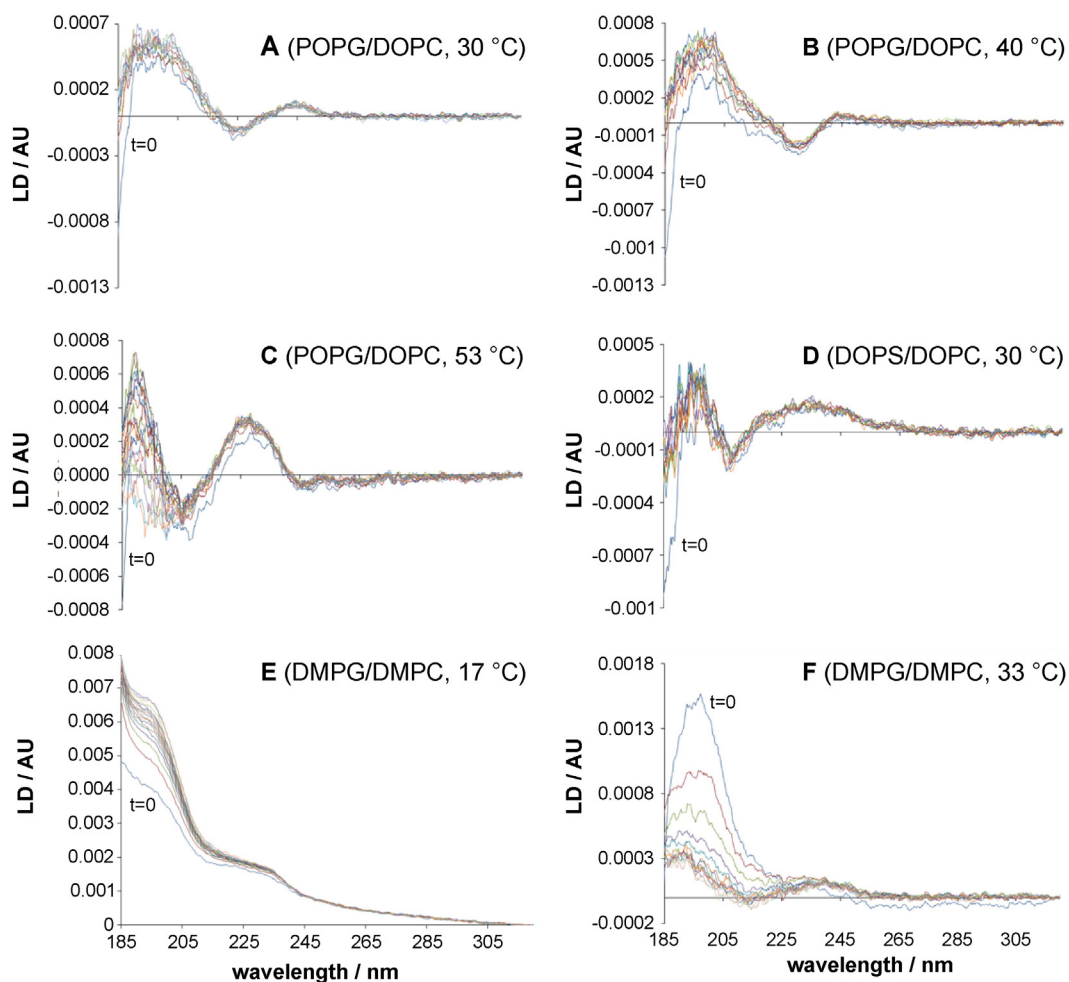


**Fig. 5.** Selected linear dichroism spectra of HNP-2 with POPG/DOPC, DOPS/DOPC or DMPG/DMPC liposomes. HNP-2 (15  $\mu$ M) was added to 50:50 (w/w) liposomes (1.4 mM). A: POPG/DOPC, 30  $^{\circ}$ C; B: POPG/DOPC, 40  $^{\circ}$ C; C: POPG/DOPC, 53  $^{\circ}$ C; D: DOPS/DOPC, 30  $^{\circ}$ C; E: DMPG/DMPC, 17  $^{\circ}$ C; F: DMPG/DMPC, 33  $^{\circ}$ C. Sixty scans were recorded at 5 min intervals; the legend in each panel shows the initial scan ( $t=0$ ).

the linear sections of the semi-log plots, the rate of the second process can be estimated to be approximately ten times slower than the first. Pseudo-first order kinetics are reasonable given the large excess of lipid and also suggest that the process does not involve multimer formation. Plots of fluorescence intensity against time and the reciprocal of fluorescence intensity against time (data not shown) ruled out zero and second order binding, as they were not linear. It was not possible to study the kinetics after 80 min by fluorescence due to the drop in signal, which was significant beyond 200 min. The reasons for this decrease are most likely a consequence of photobleaching of the fluorophore. It is notable that the equivalent semi-log plots for the evolution of LD indicate that the process is complete after approximately 100 min (Fig. 7).

Semi-log plots of the evolution of the LD signal at the wavelength of the major bands also suggested a first order binding model, with a fast initial binding stage followed by a reorientation phase (ESI). Both the fluorescence and the LD data were modelled analytically as sequential

processes, as outlined in Scheme 1. The only significant difference between the treatment of the fluorescence and LD data was the inclusion of a contribution from the fluorescence of the free peptide ( $P_f$ ) in the former case, whereas in the latter case, LD contributions are only non-zero for peptides bound to the oriented liposomes in state  $P_{m1}$  or  $P_{m2}$ . Both analytical treatments explicitly model the concentration of free peptide. It should also be noted that attempts to model the data as a two state process, with only one membrane bound state, failed to give satisfactory fits to the data. The scan speed for the fluorescence analyses was four times that of the LD analyses (200 nm/min and 50 nm/min respectively), and fluorescence spectra were recorded at 2.5 min intervals, in contrast to 5 min intervals for the LD data. Therefore, as the value for  $k_1$  determined from the fluorescence data was likely to be more accurate due to the better time resolution, initial non-linear regression was conducted using these data to determine values for  $k_1$  and  $k_2$ . The LD data were then treated with the  $k_1$  parameter fixed at the value obtained from the treatment of the fluorescence data and non-linear



**Scheme 1.** Binding model used to fit the LD and fluorescence data.

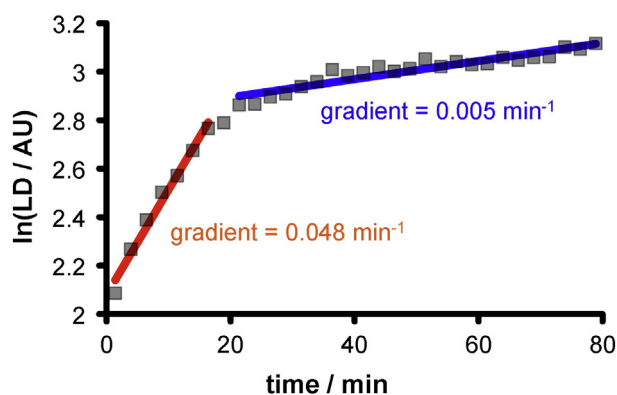


**Fig. 6.** Semi-log plot of the evolution of the fluorescence emission intensity following the addition of HNP-2 (15  $\mu\text{M}$ ) to 50:50 (w/w) POPG/DOPC liposomes (1.4 mM) at 330 nm and 30  $^{\circ}\text{C}$ . Spectra were recorded at 2.5 min intervals for 5 h.  $\lambda_{\text{exc}} = 280$  nm.

regression used to determine the remaining parameters. Using this approach, good fits to the data could be obtained in all cases (Fig. 7).

For both the fluorescence and LD data, global fits were conducted at multiple wavelengths (typically 2–5) corresponding to the most significant signals. Good fits were obtained across the range of the data (ESI) for a fast initial binding stage, represented by  $k_1$ , followed by a slower reorientation, represented by  $k_2$ . The binding model used to treat to the data implies irreversible binding of HNP-2 to the membrane. Similar irreversible kinetic models have been applied successfully to other peptides, and in others where a reversible model has been used the backwards rate constants have been found to be negligible for all stages of binding [33,41]. The rate constants and half lives determined by this treatment of the data are shown in Table 1.

The rate of formation of the initial state  $P_{m1}$  varies with the composition of the membrane, with  $k_1$  for membranes containing DMPG/

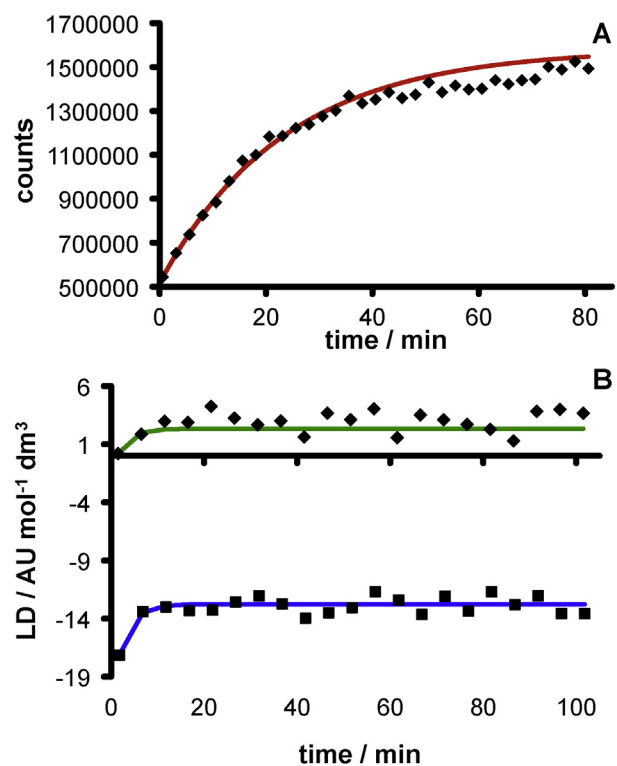


**Fig. 7.** Experimental and calculated kinetic profiles for HNP-2 binding to 50:50 (w/w) POPG/DOPC liposomes at 40  $^{\circ}\text{C}$ . A: Fluorescence emission at 330 nm; B) LD at 230 nm (squares) and 245 nm (diamonds). Experimental data are presented as points and the profiles calculated from non-linear regression as lines.

**Table 1**

Parameters calculated from non-linear least squares fitting of fluorescence and LD analyses of HNP-2 binding to liposomes using the model outlined in Scheme 1.

Lipid mixture	T/ $^{\circ}\text{C}$	$k_1/\text{min}$	$t_{1/2}/\text{min}$	$k_2/\text{min}$	$t_{1/2}/\text{min}$
POPG/DOPC	30	$2.57 \pm 0.26$	$0.27 \pm 0.03$	$0.14 \pm 0.01$	$5.06 \pm 0.51$
POPG/DOPC	40	$2.60 \pm 0.26$	$0.27 \pm 0.03$	$0.22 \pm 0.02$	$3.11 \pm 0.31$
POPG/DOPC	53	$3.43 \pm 0.34$	$0.20 \pm 0.02$	$0.19 \pm 0.02$	$3.57 \pm 0.36$
DOPS/DOPC	30	$0.73 \pm 0.07$	$0.95 \pm 0.10$	$0.23 \pm 0.02$	$3.00 \pm 0.30$
DMPG/DMPC	17	$1.40 \pm 0.14$	$0.50 \pm 0.05$	$0.05 \pm 0.01$	$14.9 \pm 1.49$
DMPG/DMPC	33	$1.03 \pm 0.10$	$0.67 \pm 0.07$	$0.12 \pm 0.01$	$5.93 \pm 0.59$

Errors are estimated as 10% from the uncertainties in the regression parameters. Repeat experiments yield data within these error limits.

DMPC being significantly slower than  $k_1$  for POPG/DOPC membranes. Inclusion of DOPS in the membrane yields the slowest rate for the initial association, which suggests that variations in the electrostatic surface potential influence binding. This also indicates that this state is likely to involve a level of membrane penetration, as the formation of an entirely peripheral disposition would be diffusion limited and not sensitive to membrane composition. In the case of membranes composed of POPG/DOPC,  $k_1$  exhibited a small increase with increasing temperature. The errors in  $k_1$  are significant when compared with the variation in  $k_1$  with temperature, and with only three data points, any assessment of the enthalpy and entropy of activation of the first binding step is qualitative. Nevertheless, the trend in  $k_1$  suggests that the enthalpy of activation ( $\Delta H^{\ddagger}$ ) for the first step is a small positive value ( $\sim 10$  kJ mol $^{-1}$ ) and the entropy of activation ( $\Delta S^{\ddagger}$ ) is negative ( $\sim -0.2$  kJ K $^{-1}$  mol $^{-1}$ ). The positive enthalpy and negative entropy of activation for the first step are consistent with a perturbation of the membrane interface by the peptide, with the relatively modest enthalpy contribution arising from the disruption of lipid–lipid interactions and the entropy component arising from the loss of degrees of freedom of the peptide. Significant desolvation would yield a positive enthalpy of activation and a positive entropy of activation. For the second step, the data do not reveal any trend sufficient to make any conclusions on the thermodynamics of the activation energy. The reorientation from  $P_{m1}$  to  $P_{m2}$ , with rate  $k_2$ , is slower in all cases than the initial binding step, which is expected for a change that involves a more significant disruption to lipid packing. Consistent with this,  $k_2$  is similar for all membranes in the fluid phase, but significantly slower in DMPG/DMPC membranes at 17  $^{\circ}\text{C}$ , which are in the gel phase at this temperature.

### 3.6. Analysis of LD spectra

For each of the membrane compositions, calculated LD spectra were generated for each of the membrane bound states of HNP-2 by iterating the regression procedure at each wavelength using the rate constants from global regression and solving for the LD values ( $LD_{m1}$  and  $LD_{m2}$ ). The spectra generated (Fig. 8) may be interpreted in terms of the transitions that generate the LD signal in order to reveal details of the binding process. The LD spectrum of HNP-2 is expected to show contributions from the transitions of  $\beta$ -sheets, tryptophan, tyrosine and phenylalanine, and possibly from the disulfide bonds. A signal from the  $\pi$ - $\pi^*$  transition of the backbone amide bonds is expected at around 195 nm. The opposing polarisations of the amide n- $\pi^*$  transition at 219 nm and 221 nm usually cancel each other out in LD spectra of  $\beta$ -sheet peptides [42]. All of the LD spectra of the two bound states of HNP-2 (Fig. 8) show peaks at 195 nm, regardless of membrane composition or temperature. The average orientation of the  $\pi$ - $\pi^*$  transitions of the backbone amide bonds is therefore parallel to the surface of the membrane.

Tryptophan has three transitions in the region between 200 and 320 nm:  $B_b$  at 220 nm,  $L_a$  at 270 nm and  $L_b$  at 280 nm. In the spectrum ( $LD_{m1}$ ) of the first membrane bound state of HNP-2 in DMPG/DMPC membranes at 33  $^{\circ}\text{C}$  (Fig. 8F), the  $B_b$  transition of tryptophan is oriented parallel to the membrane surface. In the spectrum of the second

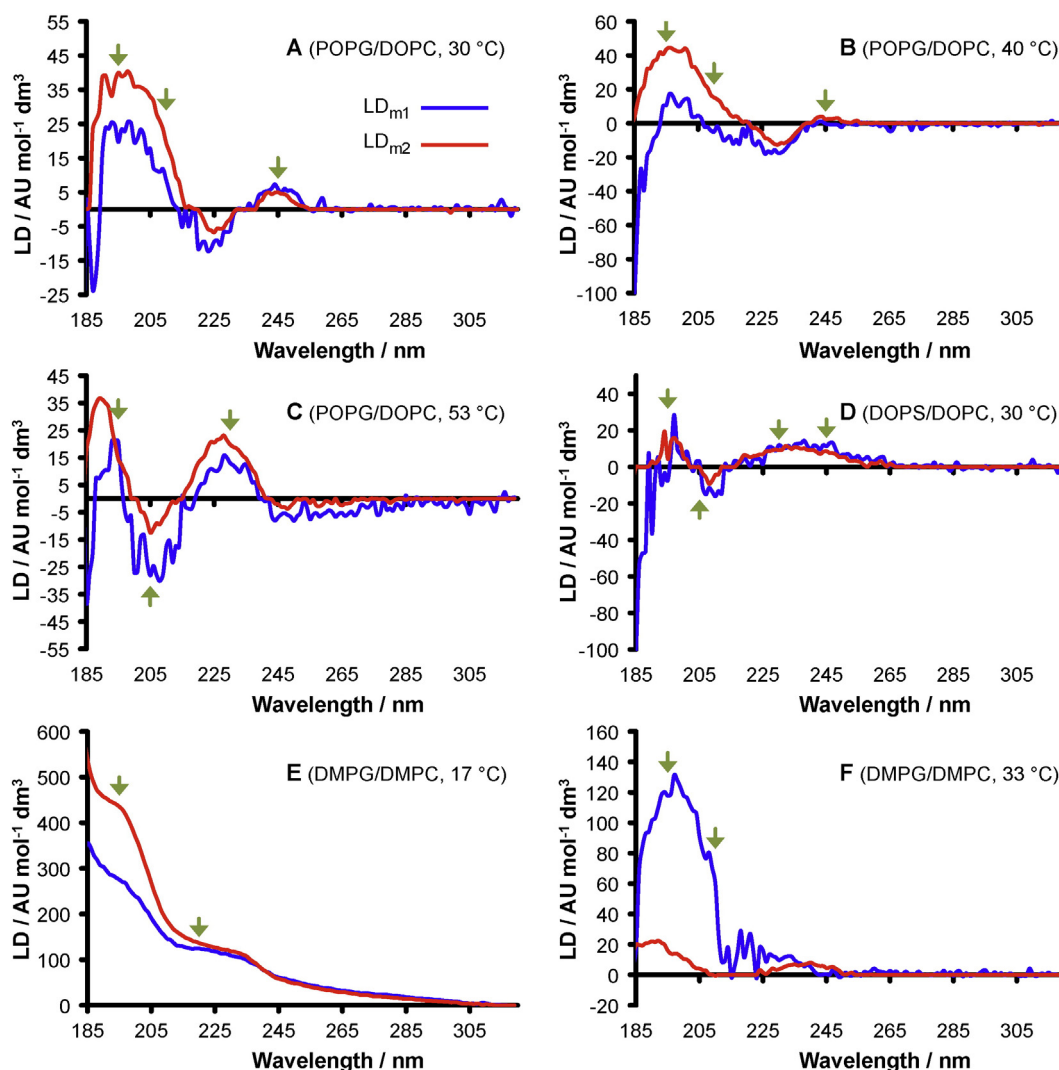


**Fig. 8.** LD profiles for the membrane bound states of HNP-2,  $LD_{m1}$  and  $LD_{m2}$ , determined by linear regression of fluorescence and LD data for the  $P_{m1}$  and  $P_{m2}$  states in 50:50 (w/w) POPG/DOPC, DOPS/DOPC or DMPG/DMPC liposomes. A: POPG/DOPC, 30 °C; B: POPG/DOPC, 40 °C; C: POPG/DOPC, 53 °C; D: DOPS/DOPC, 30 °C; E: DMPG/DMPC, 17 °C; F: DMPG/DMPC, 33 °C. Arrows indicate the positions of transitions described in the Results and discussion.

membrane bound state ( $LD_{m2}$ ) in the same lipid system, and in both membrane bound states for the POPG/DOPC membranes at 30 °C and 40 °C (Fig. 8A and B), the signal at 220 nm is zero, suggesting that the  $B_b$  transition is oriented close to 54.7° relative to the membrane normal (the magic angle), at which the LD signal is zero. There are also no clear shoulders or negative bands corresponding to the tryptophan  $B_b$  transition in DMPG/DMPC membranes at 17 °C (Fig. 8E). In the latter system, the transition is either oriented close to 54.7° relative to the membrane normal or is masked by the large amount of scattering. As discussed above, the fluorescence spectrum of HNP-2 reveals that the tryptophan residues within the dimer occupy two distinct environments due to their proximity to and interaction with tyrosine residues. Furthermore, the distance between the tryptophan and tyrosine residues was close enough for coupling to occur. This would cause a tryptophan or tyrosine transition to be split to give an in-phase and an out-of-phase contribution, which would be observed as a positive and negative band centred on the wavelength of the transition [43]. The spectra of HNP-2 in POPG/DOPC membranes at 53 °C and DOPS/DOPC membranes (Fig. 8C and D) all show splitting of the  $B_b$  transition of tryptophan due to exciton coupling to form a peak at 230 nm and a negative band at 205 nm.

The peaks attributed to exciton coupling in POPG/DOPC membranes at 53 °C and DOPS/DOPC membranes (Fig. 8C and D) at 230 nm may also incorporate a peak corresponding to the  $L_a$  transition of tyrosine

oriented parallel to the plane of the membrane. A peak or shoulder at 230 nm corresponding to the  $L_a$  band of tyrosine is observed in DMPG/DMPC membranes (Fig. 8E and F) and POPG/DOPC membranes at 30 °C and 40 °C (Fig. 8A and B). The spectra of both membrane bound states of HNP-2 in POPG/DOPC and DOPS/DOPC membranes at 30 °C (Fig. 8A and D) show peaks at 245 nm. These are attributed to the tyrosine  $L_b$  transition, which has been observed to be shifted to lower wavelengths in the spectra of peptides with a high aromatic content, oriented parallel to the membrane [44,45]. The first membrane bound state of HNP-2 in POPG/DOPC membranes at 40 °C (Fig. 8B) shows no signal at 245 nm, suggesting that the tyrosine  $L_b$  transition is oriented close to 54.7°. The spectrum of the second membrane bound state shows a weak peak at 245 nm, suggesting that the transition has reoriented towards being parallel with the surface of the membrane. For DMPG/DMPC membranes at 33 °C (Fig. 8F) a weak peak is observed in the spectrum of the second membrane bound state and no signal in the first membrane bound state. Neither of the spectra in POPG/DOPC membranes at 53 °C (Fig. 8C) shows a signal at 245 nm, and no clear peak or shoulder can be observed at 245 nm in the spectra for DMPG/DMPC membranes at 17 °C (Fig. 8E), although in the latter case any signal may be masked by scattering.

The phenylalanine  $L_a$  transition at 210 nm is expected to contribute to the LD spectrum, whereas observation of the  $L_b$  transition at 260 nm

is not expected due to its very low extinction coefficient compared to the other transitions. It is likely however, that in some cases this transition is masked by other transitions, most notably in the membranes comprising POPG/DOPC at 30 °C and 53 °C (Fig. 8A and C) and DOPS/DOPC (Fig. 8D), as well as in the first bound state in DMPG/DMPC at 33 °C (Fig. 8F). In the latter case, no signal can be observed at 210 nm in the spectrum of the second membrane bound state, suggesting that the  $L_a$  transition is oriented close to 54.7°. A negative band can be observed at 210 nm in the spectrum of the first membrane bound state in POPG/DOPC membranes at 40 °C (Fig. 8B), and a positive band in the spectrum of the second membrane bound state, suggesting that the transition reorients from parallel to the membrane to perpendicular to it when changing between the two states.

No signal can be observed from the  $L_a$  or  $L_b$  transitions of tryptophan in any of the spectra. Additionally, no clear band can be observed at 260 nm corresponding to the disulfide bonds, which is unsurprising given the weak nature of these absorptions [46]. Overall, however, the variation observed in the LD arising from aromatic side chains illustrates the rotational freedom of these residues and suggests that the orientation of these chains exhibits some independence from the backbone orientation.

All of the spectra, with the exception of those for HNP-2 association with DOPS/DOPC membranes, show significant changes in spectral form between the two membrane bound states. The spectra of HNP-2 binding to POPG/DOPC membranes at all temperatures and DMPG/DMPC membranes at 17 °C (Fig. 8A–C and E) increase in intensity between the first and second membrane bound states, indicative of a significant change in peptide orientation, but not one that involves an orthogonal change in alignment of the peptide between the plane of the membrane and the membrane normal, for which the sign of the LD would change. For POPG/DOPC membranes, there are systematic changes in the LD profile for both membrane states as the temperature is increased, with decreasing peak intensity at 210 nm and 245 nm and increasing negative band intensity at 205 nm. The origin of this trend is unclear, but may be a consequence of changes in peptide dynamics as the temperature changes, most likely a reduction in exciton coupling. There are only small changes in intensity between the spectra of the first and second membrane bound states of HNP-2 in DOPS/DOPC membranes (Fig. 8D), suggesting that either the change in orientation between the two membrane bound states is correspondingly small, or that the two membrane associated states differ by a rotation of 180° about both axes in the plane of the membrane. For DMPG/DMPC membranes at 33 °C (Fig. 8F), the spectrum of the first membrane bound state is higher in intensity when compared with systems that have DOPC as the neutral component, and the position of the maximum for the amide  $\pi$ - $\pi^*$  transition has shifted to a longer wavelength, indicating that this state has a different orientation to the DOPC systems. The second membrane bound state however, is closer to those of the POPG/DOPC membranes, indicating that the final orientation achieved in these membranes is broadly similar.

### 3.7. Assessment of binding orientations

Previous marker release experiments [47] indicate that, at the HNP-2 concentrations and lipid:peptide compositions we have used for this work, all-or-none permeabilisation of the membrane should be expected. A pore structure (Fig. 13D) has been proposed that is consistent with this poration mechanism [22]. Although these HNP-2 concentrations are considerably lower than those found *in vivo* in the oral cavity, and marginally lower than the blood plasma concentration [7], they are nevertheless likely to reflect modes by which HNP-2 exerts its antimicrobial activity. A number of models have been proposed for the structure adopted by defensins in the membranes (Fig. 9). It has been suggested, through comparison with studies on rabbit  $\alpha$ -defensins, which do not dimerise, that the features which caused HNP-2 dimer assembly are also required for the formation of the larger HNP-2 structures proposed

to be responsible for pore formation [17,18,48]. All of the models for pores revolve around the active form consisting of a dimer with a small channel through the centre of the structure. A “wedge” model involves the dimer sitting in, and disrupting, the outer leaflet of the membrane [6]. The hydrophobic base of the dimer is buried in the hydrophobic centre of the bilayer and arginine residues are able to interact with the negatively charged lipid headgroups. A “two-dimer” model involves the formation of a pore with the two dimers rotated by 90° compared to the wedge model to allow the pore to be formed by the small channel running through the centre of each dimer [6]. A “multiple dimer” model comprises a pore composed of at least four dimers arranged with polar residues facing into the centre of the pore and their hydrophobic surfaces facing outwards into the bilayer. This model has been proposed based on both the crystal structure of HNP-3 [6] and modelling of HNP-2 based on marker release experiments [22], which indicate that all-or-none leakage is induced by HNP-2 in POPG vesicles with pores large enough to allow small molecules and dextran (MW 4.4 kDa), but too small for larger dextrans (MW 19 kDa). This leads to a proposed pore composed of 6 dimers, with an internal radius of 20 Å.

Additional modes of membrane binding have been proposed to account for the fusion activity of the peptides [18]. These models propose that defensin dimers associate through the hydrophobic regions at the bases of the dimer, with the three arginine residues on each side of the dimer associating with the negatively charged lipid headgroups on the surface of the membrane, allowing two defensin dimers to associate with each other through their hydrophobic residues and with the surface of the bilayer through electrostatic interactions. The surface of another liposome is associated electrostatically with the arginine residues and the membranes are destabilised by disruption of the hydration shells surrounding them. The proposed models for the membrane binding of defensins are notable for the varying predictions of peptide orientation, where for example, the peptide backbones of the model involving a dimer of dimers sit at 90° to those of the wedge model.

LD spectra contain the information to distinguish these models. However, when the HNP-2 dimer is examined it is clear that the  $\beta$ -sheet portions are twisted and therefore the orientations of the dimer in which the  $\beta$ -sheets are oriented with the  $\pi$ - $\pi^*$  transitions mostly parallel to the membrane cannot be determined by eye. In order to obtain a better estimation of the orientation of the peptide, the experimental spectra were analysed quantitatively through fitting calculated spectra of HNP-2 in known orientations to them. The orientation of the  $\beta$ -sheet backbone in each of the two membrane bound states was determined using a set of model spectra, obtained using Dichrocalc, a program which calculates the linear dichroism spectra of peptides and proteins from oriented PDB files [36–38]. An arbitrary reference peptide orientation was established, with the “solvent pore” of the peptide aligned along the  $x$ -axis (with the  $x$ - $y$  plane corresponding to the plane of the membrane) as shown in Fig. 10. The aim of the quantitative analysis was to determine the orientations of the peptide in relation to rotations around the  $x$  and  $y$ -axes that best reproduce the experimental spectra.

LD spectra were calculated for the peptide dimer oriented as in Fig. 10 and for structures rotated by increments of 9° around either the  $x$ - or  $y$ -axis relative to this reference state. In order to take account of free rotation of the peptide about the  $z$ -axis (equivalent to the membrane normal), and the expectation that peptides could be located at any position around the cylindrical surface of a shear-deformed liposome (which aligns along the  $x$ -axis), a series of spectra obtained at 30° rotations about the  $z$ -axis and 30° tilt angles about the  $x$ -axis was averaged for each starting structure. It should be noted that our axis assignments correspond to those of Dichrocalc and differ from those used in the standard derivations for shear-aligned liposomes, where the  $z$ -axis is the long axis of the liposome. Due to the dependence of LD on the square of the cosine of the angle between a transition moment  $\mu$  and the  $z$ -axis, the data generated by rotation of each of  $\delta$  or  $\psi$  by 90°

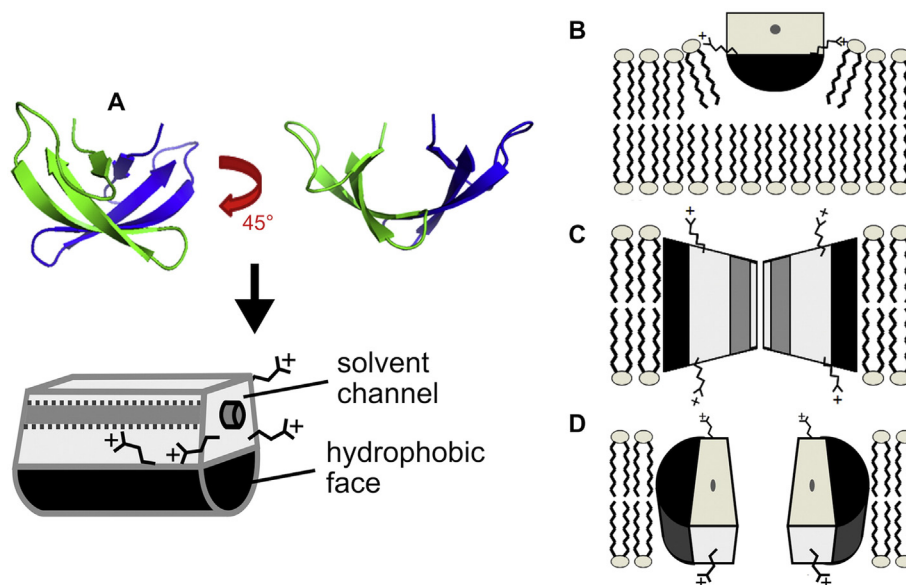


**Fig. 9.** Models proposed for the membrane binding of HNP-2 and HNP-3. A: Schematic representation of the defensin dimer; B: the wedge model; C: the two-dimer model; D: the multiple dimer model, for which two dimers are shown, but up to six have been proposed. In the original multiple dimer model [6], the solvent channel was aligned in the plane of the membrane; in the later model depicted here [22], the solvent channel is inclined at an angle of 45° to the plane of the membrane.

could be used to calculate the LD spectrum over a complete cycle of 360° (Fig. 11A).

Linear dichroism can be formalised as the difference in absorbance of light polarised parallel and perpendicular to an orientation direction. The signal is related to the polarisation of the transition relative to the orientation axis and the oscillator strength of the transition, which in our case can be expressed as  $LD = S(\mu_x^2 - \mu_y^2)$ , where  $\mu_x$  and  $\mu_y$  are the components of the transition dipole along the  $x$ - and  $y$ -axes respectively and  $S$  is a scaling factor that reflects proportion of the liposomes that are aligned as a cylinder. In our case, changing the angle  $\delta$  from the reference state in increments of 9° whilst leaving  $\psi$  at the reference value enabled the  $y$ -axis component at each wavelength ( $\mu_y$ ) to be determined by fitting Eq. (7) to the calculated LD value. Similarly, the  $x$ -axis component ( $\mu_x$ ) was determined using Eq. (8) from increments in  $\psi$  with  $\delta$  at the reference value. With knowledge of both  $\mu_x$  and  $\mu_y$  at each

wavelength, it was then possible to calculate the LD value for any combination of  $\delta$  and  $\psi$  using Eq. (9) (Fig. 11B–D). The values of  $\delta$  and  $\psi$  that gave the best fit to the calculated spectrum were obtained by regression. This analysis was restricted to backbone amide transitions in the range 187 nm to 205 nm. This was justified on the grounds that side chain rotamers in the membrane associated states may differ significantly from the crystal structure of HNP-2, and as discussed above exhibit greater conformational flexibility. Furthermore, Dichrocalc did not reproduce the exciton coupling observed experimentally. An interesting feature of Eq. (9) is that the position of the maximum between 187 nm and 205 nm has a greater influence on the optimal  $\delta/\psi$  combination than the magnitude of the LD. The magnitude of the LD is captured by the parameter  $S'$ . This is demonstrated well by the fit obtained for DMPG/DMPC at 33 °C, where the  $\delta/\psi$  combination for the  $P_{m1}$  state yields an intrinsically lower LD than the  $P_{m2}$  state, despite the reverse being observed experimentally. The much higher experimental value for  $P_{m1}$  is reflected by a higher value for  $S'$ , which is presumably a consequence of a higher proportion of liposomes aligned by shear flow in the  $P_{m1}$  state.

The experimental LD profiles in Fig. 8 represent time-averaged structures and are subject to both systematic errors in the measurements and errors resulting from regression. The calculated profiles in Fig. 11 have been generated from a single static structure and therefore do not encapsulate dynamic conformational changes in the peptide. As a consequence, the errors in  $\delta$  and  $\psi$  for the best fit of the calculated to the experimental data are significant. An additional inherent feature of the LD spectra generated by iterations over the full range of  $\delta$  and  $\psi$  is that there are two values for each (separated by 180°) that give an identical solution, yielding two pairs of  $\delta/\psi$  combinations in total with the same LD profile. An example is given in Fig. 11B for each of the  $P_{m1}$  and  $P_{m2}$  states in the DMPG/DMPC system, in which members of a given pair have a diagonal relationship in the plot. Within each pair, the effective orientation is the same due to averaging about the  $z$ -axis. Between pairs, the orientations differ by changing one, but not both, of  $\delta$  or  $\psi$ . Some general points can be made. The range of LD values for rotations about the  $y$ -axis ( $\psi$ ) is significantly smaller than those about the  $x$ -axis, which is to be expected as the former maintain the long axis of the peptide in the plane of the membrane, whereas the latter involve configurations (at  $\delta = 90^\circ$  and  $270^\circ$ ) where the long axis of the peptide is aligned along the membrane normal. As all of the experimental LD

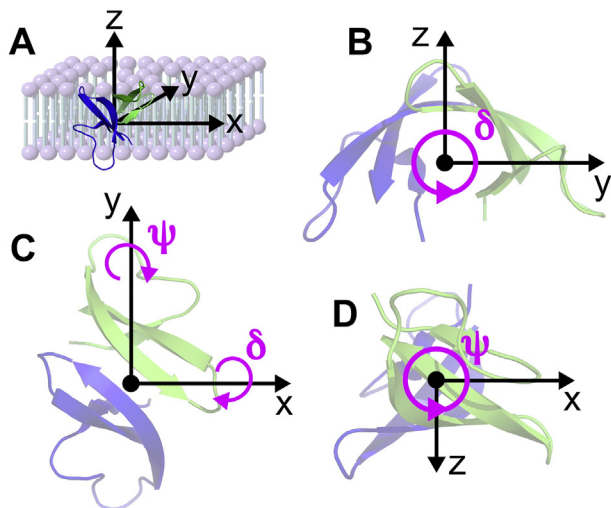


**Fig. 10.** The orientation of the HNP-2 dimer in the reference state. A depicts the orientation of HNP-2 with regard to the axis system, and the alignment of the axis system with a lipid bilayer. B, C and D show respectively the view looking down the  $x$ -,  $z$ - and  $y$ -axes towards the origin. PDB ID 1DFN was used as the template structure, with the “solvent channel” aligned along the  $x$ -axis. The plane of the membrane corresponds to the  $x$ - $y$  plane;  $\delta$  denotes the rotation about the  $x$ -axis and  $\psi$  about the  $y$ -axis.

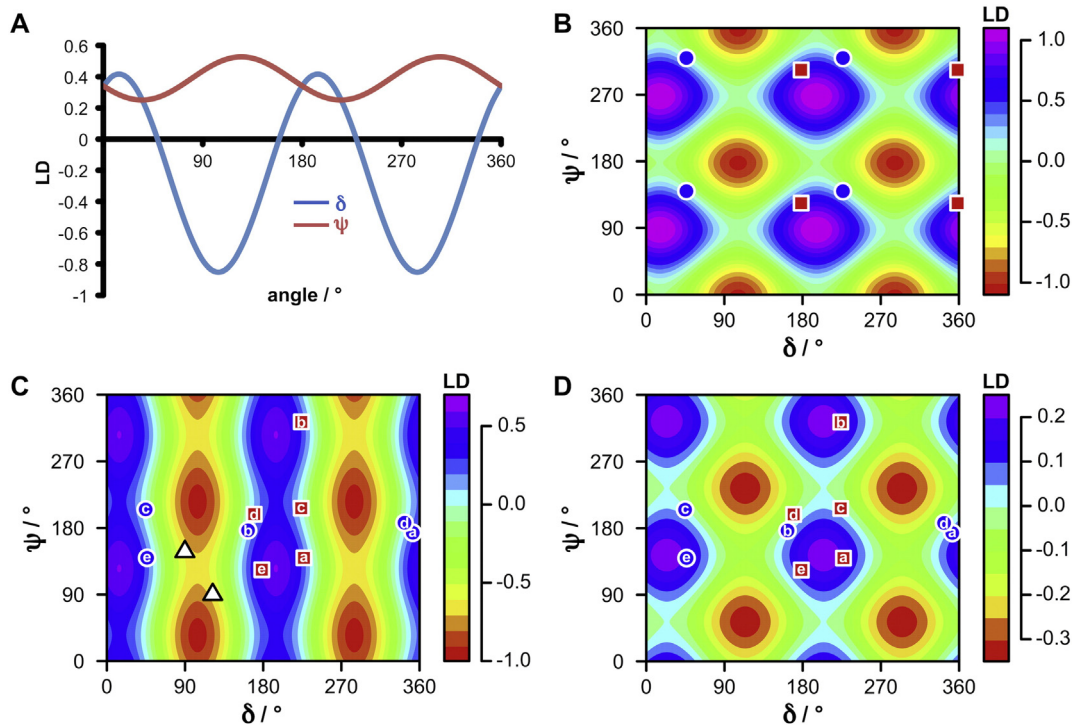


**Fig. 11.** LD profiles for HNP-2 generated by iterations over  $\delta$  and  $\psi$ . A: The LD signal at 195 nm for changes in  $\delta$  ( $\psi = 0^\circ$ ) and  $\psi$  ( $\delta = 0^\circ$ ); B: contour plot showing the LD profile for combinations of  $\delta$  and  $\psi$  at 187 nm. Superimposed on this plot are the 4 identical best fits for each of  $P_{m1}$  and  $P_{m2}$  in the DMPG/DMPC system at 33 °C; C: LD profile for combinations of  $\delta$  and  $\psi$  at 195 nm; D: LD profile for combinations of  $\delta$  and  $\psi$  at 205 nm. In each case,  $P_{m1}$  configurations are indicated by blue circles and  $P_{m2}$  configurations by red squares. In panels C and D only one of the four  $\delta/\psi$  combinations is shown in each case and lowercase characters correspond to a: POPG/DOPC at 30 °C; b: POPG/DOPC at 40 °C; c: DOPG/DOPC at 53 °C; d: DOPS/DOPC; and e: DMPG/DMPC at 33 °C. In panel C,  $\delta/\psi$  combinations for a multiple dimer pore are indicated by triangles. LD is in extinction coefficient units.

spectra in Fig. 8 have positive LD signals at 195 nm, it is apparent from the contour plot in Fig. 11C that this restricts  $\delta$  to values in the region of  $0^\circ$  or  $180^\circ$ , which correspond to a configuration close to the reference state (Fig. 10) and the reference state rotated by  $180^\circ$  about the  $x$ -axis. The latter configuration is close to that of the wedge model (Fig. 9B). The two dimer model (Fig. 9C) is related to the reference structure by  $\delta = 0^\circ$  and  $\psi = 90^\circ$ , for which a strongly positive LD at 187 nm, positive LD at 195 nm and weakly positive LD at 205 nm would be expected. These criteria are met by most of the LD spectra for the  $P_{m2}$  state, as well as  $P_{m1}$  for the DMPG/DMPC system at 33 °C. The multiple dimer model (Fig. 9D) is related to the reference structure by two  $\delta/\psi$  combinations (Fig. 11C):  $\delta = 90^\circ$ ,  $\psi = 148^\circ$ ; and  $\delta = 122^\circ$ ,  $\psi = 90^\circ$ . For both of these, a strongly negative LD at 195 nm would be expected, which is not observed experimentally.

Changes in the LD spectrum between the  $P_{m1}$  and  $P_{m2}$  states can in principle result from a move between any of the pairs of solutions for  $P_{m1}$  and  $P_{m2}$ . For all membranes containing DOPC, with values of  $\delta$  or  $\psi$  for  $P_{m1}$  that are remarkably similar and close to  $0^\circ$  and  $180^\circ$ , this would suggest, as noted above, that the peptide in  $P_{m1}$  is oriented close to the reference structure, or with  $\delta$  or  $\psi$  rotated by  $180^\circ$  (Fig. 13A). Analysis of the surface potential of the HNP-2 dimer reveals that the peptide has the overall shape of a spherical wedge, with the convex surface (Fig. 12A) having a significantly greater area of positive potential than the faces (Fig. 12B, C). As electrostatic interactions are a prerequisite for HNP-2 association with membranes, it is reasonable to suggest that the convex surface makes the first contact with the membrane surface to form  $P_{m1}$ .

In both of the pairs of solutions for the  $P_{m2}$  state in the membranes containing DOPC, the dimer adopts a skewed configuration in which a significant proportion of the  $\beta$ -sheet from one of the monomers is aligned in the plane of the membrane, with the axis normal to the sheet surface also aligned in the same plane (Fig. 13B). The  $\beta$ -sheet of the other monomer twists away from the  $x$ - $y$  plane and is therefore

only partly aligned with the plane of membrane. This configuration is particularly interesting as it is related to the multiple dimer pore (Fig. 13D) by a single rotation about the  $x$ -axis of  $30^\circ$ , and is therefore consistent with a multiple dimer model in which the axis of the pore is tilted away from the normal by  $30^\circ$ , rather than the ideal structure presented in Fig. 13D. Such a tilted structure can be rationalised if there is a mismatch between the height of the pore and the distance between the phosphate regions of the bilayer, on the basis that it would then maximise the potential for electrostatic contacts between the components of the pore and the PG headgroups.

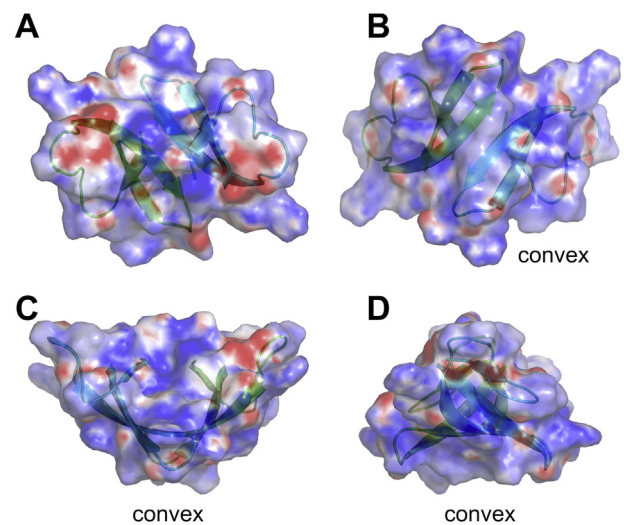


**Fig. 12.** The electrostatic surface potential of HNP-2. Negative potential = red; positive potential = blue; contoured from  $-10$  to  $10$  kT/e. A: The surface distal to the convex surface; B: the convex surface; C: face view; D: end view.

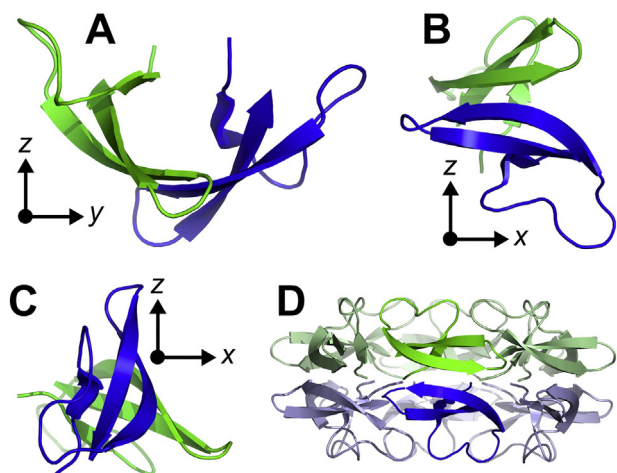


**Fig. 13.** Exemplar configurations arising from fitting simulated LD spectra to the experimental LD data for POPG/DOPC (average for data at 30 °C and 40 °C) and DMPG/DMPC membranes at 33 °C. A:  $P_{m1}$  state for POPG/DOPC; B:  $P_{m2}$  state for POPG/DOPC; C:  $P_{m2}$  state for DMPG/DMPC; D: the multiple dimer model [22] for comparison (in the same orientation as B and C). In all cases, the view is in the plane of the membrane (which corresponds to the  $x$ - $y$  plane). See the ESI for details of all configurations generated by this process.

In DMPG/DMPC membranes at 33 °C, the  $P_{m1}$  state is almost identical to the  $P_{m2}$  state in POPG/DOPC at 30 °C and 40 °C (Fig. 13B). Two scenarios may account for failure to observe a wedge orientation: either the wedge orientation is disfavoured in DMPG/DMPC membranes and does not form, or the wedge orientation forms, but is rapidly converted into the skewed/pore configuration. These two possibilities cannot be resolved using our data. The  $P_{m2}$  state in DMPG/DMPC is characterised by a rotation around the  $y$ -axis that places one side of the spherical wedge into the  $x$ - $y$  plane (Fig. 13C). Whether this configuration has any functional significance is uncertain. Taken together, it is apparent that there is a small but finite number of favourable orientations for the peptide in the membrane, and the orientation preferentially adopted by the peptide is sensitive to the acyl chain composition of the membrane. The reasons for this sensitivity are likely to be a complex balance of a number of factors, such as the flexibility and compressibility of the membrane, the area per lipid headgroup and the extent of hydration of the membrane interface.

#### 4. Conclusions

In this work we have shown that a combination of LD and fluorescence spectroscopies can be used to determine the binding kinetics of the human host defence peptide HNP-2 with model membranes. Analysis of the combined data using an analytical model for the association kinetic data reveals that the binding is a two stage process, with a fast initial step followed by a slower reorientation. Predicted spectra for each of the bound states, when interpreted alongside simulated spectra, reveal that the wedge model is the initial binding configuration in POPG/POPC membranes, but not DMPG/DMPC. In POPG/POPC membranes, the peptides reorient to a configuration that is similar to the multiple pore model, but skewed from the idealised pore orientation by 30°. This latter configuration also corresponds to the initial bound state in DMPG/DMPC membranes. In DMPG/DMPC membranes, an additional mode of binding is produced by reorientation to an alignment of the peptide dimer in which one face of the wedge is aligned more in the plane of the membrane.

#### Transparency document

The Transparency document associated with this article can be found in online version.

#### Acknowledgements

The authors thank the EPSRC (EP/P502438/1) for funding.

#### Appendix A

The axis system that we have used in this article, with the  $z$ -axis corresponding to the membrane normal and the  $x$ -axis corresponding to the axis of the cylinder of a shear-deformed liposome, differs from the standard axis system commonly referred to when discussing LD experiments, where the  $z$ -axis is the axis of the liposome and the  $x$ -axis normal to membrane surface [29]. This is due to the different axis systems used by Dichrocalc. Dichrocalc uses the standard LD equation (Eq. (A.1))

$$LD^r = \frac{3}{2}S(3\cos^2\beta - 1) \quad (\text{A.1})$$

where  $\beta$  is the angle between the transition polarisation direction and the flow direction and  $LD^r$  is the reduced LD. For analyses of binding to liposomes Eq. (A.2) is appropriate

$$LD^r = \frac{3}{4}S(1 - 3\cos^2\alpha) \quad (\text{A.2})$$

where  $\alpha$  is the angle between the membrane normal and the polarisation direction [49]. The orienting force on the peptide is the membrane, which is perpendicular to the flow direction. A graphical depiction of the Dichrocalc setup is presented in the ESI. In order to interpret the Dichrocalc results correctly the spectra produced by the Dichrocalc calculations were therefore inverted.

#### Appendix B. Supplementary data

Supplementary data to this article can be found online at <http://dx.doi.org/10.1016/j.bbmem.2016.01.014>.

#### References

- [1] S. Mukherjee, L.V. Hooper, Antimicrobial defense of the intestine, *Immunity* 42 (2015) 28–39.
- [2] H. Chen, Z. Xu, L. Peng, X. Fang, X. Yin, N. Xu, P. Cen, Recent advances in the research and development of human defensins, *Peptides* 27 (2006) 931–940.
- [3] T. Ganz, *Nat. Rev. Immunol.* 3 (2003) 710–720.
- [4] J.J. Schneider, A. Unholzer, M. Schaller, M. Schäfer-Korting, H.C. Korting, Human defensins, *J. Mol. Med.* 83 (2005) 587–595.
- [5] J. Wiesner, A. Vilcinskis, Antimicrobial peptides: the ancient arm of the human immune system, *Virulence* 1 (2010) 440–464.
- [6] C.P. Hill, J. Yee, M.E. Selsted, D. Eisenberg, Crystal structure of defensin HNP-3, an amphiphilic dimer: mechanisms of membrane permeabilization, *Science* 251 (1991) 1481–1485 (PDB ID: 1DFN).
- [7] R.I. Lehrer, W. Lu,  $\alpha$ -Defensins in human innate immunity, *Immunol. Rev.* 245 (2012) 84–112.
- [8] A. van Dijk, E.J.A. Veldhuizen, H.P. Haagsman, Avian defensins, *Vet. Immunol. Immunopathol.* 124 (2008) 1–18.
- [9] C. Xie, A. Prah, B. Ericksen, Z. Wu, P. Zeng, X. Li, W.-Y. Lu, J. Lubkowski, W. Lu, Reconstruction of the conserved beta-bulge in mammalian defensins using D-amino acids, *J. Biol. Chem.* 280 (2005) 32921–32929.
- [10] A. Pardi, X.L. Zhang, M.E. Selsted, J.J. Skalicky, P.F. Yip, NMR studies of defensin antimicrobial peptides 2 three-dimensional structures of rabbit NP-2 and human HNP-1, *Biochemistry* 31 (1992) 11357–11364.
- [11] X.L. Zhang, M.E. Selsted, A. Pardi, NMR studies of defensin antimicrobial peptides 1 resonance assignment and secondary structure determination of rabbit NP-2 and human HNP-1, *Biochemistry* 31 (1992) 11348–11356.
- [12] A. Szyk, Z. Wu, K. Tucker, D. Yang, W. Lu, J. Lubkowski, Crystal structures of human alpha-defensins HNP4, HD5, and HD6, *Protein Sci.* 15 (2006) 2749–2760.
- [13] M. Pazgier, G. Wei, B. Ericksen, G. Jung, Z. Wu, E. de Leeuw, W. Yuan, H. Szmanski, W.-Y. Lu, J. Lubkowski, R.I. Lehrer, W. Lu, Sometimes it takes two to tango: contributions of dimerization to functions of human  $\alpha$ -defensin HNP1 peptide, *J. Biol. Chem.* 287 (2012) 8944–8953.
- [14] Y. Zhang, T. Doherty, J. Li, W. Lu, C. Barinka, J. Lubkowski, M. Hong, Resonance assignment and three-dimensional structure determination of a human alpha-defensin, HNP-1, by solid-state NMR, *J. Mol. Biol.* 397 (2010) 408–422.
- [15] M.E. Selsted, S.S. Harwig, T. Ganz, J.W. Schilling, R.I. Lehrer, Primary structures of three human neutrophil defensins, *J. Clin. Invest.* 76 (1985) 1436–1439.

- [16] S. Cociancich, A. Ghazi, C. Hetru, J.A. Hoffmann, L. Letellier, Insect defensin, an inducible antibacterial peptide, forms voltage-dependent channels in *Micrococcus luteus*, *J. Biol. Chem.* 268 (1993) 19239–19245.
- [17] K. Hristova, M.E. Selsted, S.H. White, Interactions of monomeric rabbit neutrophil defensins with bilayers: comparison with dimeric human defensin HNP-2, *Biochemistry* 35 (1996) 11888–11894.
- [18] G. Fujii, M.E. Selsted, D. Eisenberg, Defensins promote fusion and lysis of negatively charged membranes, *Protein Sci.* 2 (1993) 1301–1312.
- [19] J. Kim, M. Mosior, L.A. Chung, H. Wu, S. McLaughlin, Binding of peptides with basic residues to membranes containing acidic phospholipids, *Biophys. J.* 60 (1991) 135–148.
- [20] W.C. Wimley, S.H. White, Quantitation of electrostatic and hydrophobic membrane interactions by equilibrium dialysis and reverse-phase HPLC, *Anal. Biochem.* 213 (1993) 213–217.
- [21] W. Kabsch, C. Sander, *Biopolymers* 22 (1983) 2577–2637.
- [22] W.C. Wimley, M.E. Selsted, S.H. White, Interactions between human defensins and lipid bilayers: evidence for formation of multimeric pores, *Protein Sci.* 3 (1994) 1362–1373.
- [23] R.I. Lehrer, A. Barton, K.A. Daher, S.S. Harwig, T. Ganz, M.E. Selsted, Interaction of human defensins with *Escherichia coli* mechanism of bactericidal activity, *J. Clin. Invest.* 84 (1989) 553–561.
- [24] A.M. Cole, T. Ganz, A.M. Liese, M.D. Burdick, L. Liu, R.M. Strieter, Cutting edge: IFN-inducible ELR-CXC chemokines display defensin-like antimicrobial activity, *J. Immunol.* 167 (2001) 623–627.
- [25] Y. Wu, H.W. Huang, G.A. Olah, Method of oriented circular dichroism, *Biophys. J.* 57 (1990) 797–806.
- [26] W. Hohlweg, S. Kosol, K. Zangger, Determining the orientation and localization of membrane-bound peptides, *Curr. Protein Pept. Sci.* 13 (2012) 267–279.
- [27] M.R. Hicks, J. Kowalski, A. Rodger, LD spectroscopy of natural and synthetic biomaterials, *Chem. Soc. Rev.* 39 (2010) 3380–3393.
- [28] A. Rodger, R. Murrington, M.A. Geeves, M. Hicks, L. de Alwis, D.J. Halsall, T.R. Dafforn, Looking at long molecules in solution: what happens when they are subjected to Couette flow? *Phys. Chem. Chem. Phys.* 8 (2006) 3161–3171.
- [29] A. Rodger, J. Rajendra, R. Murrington, M. Ardammar, B. Nord'en, J.D. Hirst, A.T.B. Gilbert, T.R. Dafforn, D.J. Halsall, C.A. Woolhead, C. Robinson, T.J.T. Pinheiro, J. Kazlauskaitė, M. Seymour, N. Perez, M.J. Hannon, Flow oriented linear dichroism to probe protein orientation in membrane environments, *Phys. Chem. Chem. Phys.* 4 (2002) 4051–4057.
- [30] R. Murrington, T.R. Dafforn, D.J. Halsall, J.I. MacDonald, M. Hicks, A. Rodger, Validation of new microvolume Couette flow linear dichroism cells, *Analyst* 130 (2005) 1608–1616.
- [31] T.R. Dafforn, J. Rajendra, D.J. Halsall, L.C. Serpell, A. Rodger, Protein fiber linear dichroism for structure determination and kinetics in a low-volume, low-wavelength Couette flow cell, *Biophys. J.* 86 (2004) 404–410.
- [32] A. Damianoglou, A. Rodger, C. Pridmore, T.R. Dafforn, J.A. Mosely, J.M. Sanderson, M.R. Hicks, The synergistic action of melittin and phospholipase A2 with lipid membranes: development of linear dichroism for membrane-insertion kinetics, *Protein Pept. Lett.* 17 (2010) 1351–1362.
- [33] S.M. Ennaceur, M.R. Hicks, C.J. Pridmore, T.R. Dafforn, A. Rodger, J.M. Sanderson, Peptide adsorption to lipid bilayers: slow processes revealed by linear dichroism spectroscopy, *Biophys. J.* 96 (2009) 1399–1407.
- [34] C.E.B. Caesar, E.K. Esbjorner, P. Lincoln, B. Norden, Membrane interactions of cell-penetrating peptides probed by tryptophan fluorescence and dichroism techniques: correlations of structure to cellular uptake, *Biochemistry* 45 (2006) 7682–7692.
- [35] E. Gasteiger, C. Hoogland, A. Gattiker, S. Duvaud, M.R. Wilkins, R.D. Appel, A. Bairoch, Protein identification and analysis tools on the ExPASy server, in: J.M. Walker (Ed.), *The Proteomics Protocols Handbook*, Humana Press 2005, pp. 571–607.
- [36] B.M. Bulheller, J.D. Hirst, DichroCalc—circular and linear dichroism online, *Bioinformatics* 25 (2009) 539–540.
- [37] N.A. Besley, J.D. Hirst, Theoretical studies toward quantitative protein circular dichroism calculations, *J. Am. Chem. Soc.* 121 (1999) 9636–9644.
- [38] M.T. Oakley, J.D. Hirst, Charge-transfer transitions in protein circular dichroism calculations, *J. Am. Chem. Soc.* 128 (2006) 12414–12415.
- [39] J.T. Vivian, P.R. Callis, Mechanisms of tryptophan fluorescence shifts in proteins, *Biophys. J.* 80 (2001) 2093–2109.
- [40] P.N. Yi, R.C. MacDonald, Temperature dependence of optical properties of aqueous dispersions of phosphatidylcholine, *Chem. Phys. Lipids* 11 (1973) 114–134.
- [41] J. Tang, H. Yin, J. Qiu, M.J. Tucker, W.F. DeGrado, F. Gai, Using two fluorescent probes to dissect the binding, insertion, and dimerization kinetics of a model membrane peptide, *J. Am. Chem. Soc.* 131 (2009) 3816–3817.
- [42] T.R. Dafforn, A. Rodger, Linear dichroism of biomolecules: which way is up? *Curr. Opin. Struct. Biol.* 14 (2004) 541–546.
- [43] E. Esbjorner, C. Caesar, B. Albinsson, P. Lincoln, B. Norden, Tryptophan orientation in model lipid membranes, *Biochem. Biophys. Res. Commun.* 361 (2007) 645–650.
- [44] M.C. Wiener, S.H. White, Structure of a fluid dioleoylphosphatidylcholine bilayer determined by joint refinement of X-ray and neutron diffraction data. III Complete structure, *Biophys. J.* 61 (1992) 434–447.
- [45] L.H. Greene, E.D. Chrysina, L.I. Irons, A.C. Papageorgiou, K.R. Acharya, K. Brew, Role of conserved residues in structure and stability: tryptophans of human serum retinol-binding protein, a model for the lipocalin superfamily, *Protein Sci.* 10 (2001) 2301–2316.
- [46] G.D. Fasman, *Circular Dichroism and the Conformational Analysis of Biomolecules*, Plenum Press, New York, USA, 1996.
- [47] A.S. Ladokhin, W.C. Wimley, S.H. White, Leakage of membrane vesicle contents: determination of mechanism using fluorescence quenching, *Biophys. J.* 69 (1995) 1964–1971.
- [48] K. Hristova, M.E. Selsted, S.H. White, Critical role of lipid composition in membrane permeabilization by rabbit neutrophil defensins, *J. Biol. Chem.* 272 (1997) 24224–24233.
- [49] B.M. Bulheller, A. Rodger, J.D. Hirst, Circular and linear dichroism of proteins, *Phys. Chem. Chem. Phys.* 9 (2007) 2020–2035.